

Learning Non-linear Wavelet Transformation via Normalizing Flow

Shuo-Hui Li¹

Abstract

Wavelet transformation stands as a cornerstone in modern data analysis and signal processing. Its mathematical essence is an invertible transformation that discerns slow patterns from fast patterns in the frequency domain, which repeats at each level. Such an invertible transformation can be learned by a designed normalizing flow model. With a factor-out scheme resembling the wavelet downsampling mechanism, a mutually independent prior, and parameter sharing along the depth of the network, one can train normalizing flow models to factor-out variables corresponding to fast patterns at different levels, thus extending linear wavelet transformations to non-linear learnable models. In this paper, a concrete way of building such flows is given. Then, a demonstration of the model's ability in lossless compression task, progressive loading, and super-resolution (up-sampling) task. Lastly, an analysis of the learned model in terms of low-pass/high-pass filters is given.

1. Introduction

The applications of wavelet transformation are pervasive, ranging from image processing, like edge detection (Canny, 1986; Marr & Hildreth, 1980; Mallat & Hwang, 1992), watermarking (Dugad et al., 1998) and image morphing (He et al., 1994), to data manipulations like denoising (Donoho, 1992; Donoho & Johnstone, 1994) and data compression (Rabbani, 2002; Charrier, 1999), and to numerical analysis, like solving ODEs and PDEs (Sweldens, 1994; Cruz et al., 2001). As deep learning techniques advance to domain-specific areas, wavelet transformation has also been used in these machine learning tasks. For example, super-resolution

¹Institute of Physics, Chinese Academy of Sciences, Beijing, China. Correspondence to: Shuo-Hui Li <contact_lish@iphy.ac.cn>.



Figure 1. Two iterations of the learned wavelet transformation, normalizations are performed for each channel for visualization. The transformation is trained on the ImageNet64 dataset and evaluated on the Lena image(512×512).

task (Yu et al., 2020; Zhong et al., 2018; Huang et al., 2017), image generation task (Ardizzone et al., 2019), image segmentation task (Figueiredo, 2005), and signal analysis (Amin et al., 2015; Chen et al., 2015; Shafiullah et al., 2017). Also, there are attempts to enhance deep learning with wavelets, such as propose a better pooling mechanism (Williams & Li, 2018), and using wavelets to analyze training datasets (Yousefzadeh & Huang, 2020). Powerful as they are, wavelet transformations have several unfavorable merits. They are linear transformations, allowing simple adding/subtracting manipulations, but limits their expressive ability. They are derived using mathematical constraints, applicable to nearly all datasets, which, however, prevents them to be tailored to specific tasks on specific datasets.

Normalizing flows, on the other hand, are a family of non-linear invertible deep learning models (Dinh et al., 2015; 2016; Kingma & Dhariwal, 2018; Chen et al., 2018; Li et al., 2020; Li & Wang, 2018). Their applications

cover many topics, including image generation (Kingma & Dhariwal, 2018; Dinh et al., 2016), independent component analysis (ICA) (Dinh et al., 2015; Sorrenson et al., 2020), variational inference (Kingma et al., 2016b; Rezende & Mohamed, 2015), Monte Carlo sampling (Song et al., 2017), and scientific applications (Li et al., 2020; Li & Wang, 2018; Hu et al., 2020a; Noé et al., 2019). Normalizing flows are a promising candidate for learnable wavelet transformation. They share many common features with wavelet transformations. The two are both invertible transformations, and Normalizing flows have a proven ability to discern frequency patterns (Dinh et al., 2015; Sorrenson et al., 2020; Li et al., 2020; Li & Wang, 2018). Some kinds of normalizing flows even have a factor-out scheme (Li & Wang, 2018; Dinh et al., 2016; Hoogeboom et al., 2019), which resembles downsampling in wavelet transformations.

Building on the inherent connection between wavelet transformation and normalizing flow, this paper proposes a learnable wavelet transformation model. In this proposed model, a fact-out scheme that is adapted from wavelet transformation’s downsampling is used. The factored-out variables are considered from mutually independent distributions for them to be fast-frequency variables. And parameters are shared along the depth of the network, to make sure each layer is performing the same transformation. As a normalizing flow model, the proposed model requires fewer parameters, thus has better generalization ability and smaller computation expense. The parameters-sharing scheme also relaxes dimensional constraints, allowing the model to be performed on different sample sizes than trained on. It’s also a natural fit for traditional wavelet tasks like lossless compression, super-resolution, and so on. As a wavelet transformation, it’s trained to fit its task purpose and datasets. It’s also a non-linear transformation, which grants it more expressive power in complex tasks.

This paper is organized as follows. Sec. 2 gives an introduction of the background, drawing connections between wavelet and flow models. Sec. 3 shows the exact scheme of constructing a learnable wavelet flow. Sec. 4 demonstrates the model’s performance in lossless compression, progressive loading, and super-resolution task. And numerically analysis the learned filters. Sec. 5 gives a brief review of related works. Finally, Sec. 6 concludes the paper.

2. Background

This section introduces two fundamental concepts, the normalizing flow and discrete wavelet transformation.

2.1. Normalizing Flow

Normalizing Flows are a family of parameterized bijective mappings. The core feature of these bijective mappings is their tractable probability change. For a bijective mapping $f : \mathcal{X} \rightarrow \mathcal{Z}$, its probability change can be described as

$$P_{\mathcal{X}}(x) = P_{\mathcal{Z}}(z) \left| \det \left(\frac{\partial z}{\partial x} \right) \right| \quad (1)$$

where $P_{\mathcal{X}}(x)$ and $P_{\mathcal{Z}}(z)$ are probabilities of variable x and z respectively. Normalizing flows usually have an easy-to-compute determinant, thus a tractable probability.

One concrete example of such a network is the Non-linear Independent Component Estimate(NICE) (Dinh et al., 2015), whose f formulates as follows,

$$\begin{aligned} \mathbf{z}_A &= \mathbf{x}_A + t(\mathbf{x}_B) \\ \mathbf{z}_B &= \mathbf{x}_B \end{aligned} \quad (2)$$

where variable \mathbf{z} is divided into two parts, $\mathbf{z} = (\mathbf{z}_A, \mathbf{z}_B)$, and so does variable \mathbf{x} . t here stands for an arbitrary parameterized transformation that maps \mathbf{x}_B to the space of \mathbf{x}_A . This transformation f is easily invertible, thus a bijective mapping. The role of \mathbf{x}_A and \mathbf{x}_B can be reversed at the next layer to make changes to all variables of \mathbf{x} . One can see that the Jacobian determinant of such transformation is exactly 1, meaning this kind of transformation preserves the probability.

In some kinds of normalizing flow implementations(Li & Wang, 2018; Dinh et al., 2016; Hoogeboom et al., 2019), a mechanism called factor-out is used. When factor-out is performed, part of the variables are kept from later transformations, and leave as it is to concatenate with the resulting other parts of variables after the last layer, forming the final transformed variables. After factor-out, the dimension of variables to be transformed is shrunk. In some works, this shrinkage of dimension can be utilized to discern fast-frequency patterns (Li & Wang, 2018; Hu et al., 2020b).

As bijective mappings form a group, so does normalizing flows. We can chain these layers and use a factor-out scheme to form hierarchical-structure normalizing flow models. This gives us a way to come up with complex, designed normalizing flows.

2.2. Discrete Wavelet Transformation

Discrete wavelet transformations are essentially invertible linear transformations. These transformations are usually formed by two kinds of filters, the low-pass filters \mathbf{H} and the high-pass filters \mathbf{G} . We can write them

as different rows in a single transformation matrix \mathbf{W} . Then the transformation can be formulated as follows.

$$\mathbf{y} = \mathbf{W}\mathbf{x} = \begin{bmatrix} \mathbf{H}\mathbf{x} \\ \mathbf{G}\mathbf{x} \end{bmatrix} \quad (3)$$

where \mathbf{y} and \mathbf{x} are one-dimensional vectors. This linear transformation is followed by a downsampling operation. After downsampling, only low-pass filter results $\mathbf{H}\mathbf{x}$ are kept. This linear transformation with downsampling is called one iteration of the wavelet transformation. And the next iteration of wavelet transformation will be on the low-pass filter results.

For two-dimensional data, one can apply the transformation matrix twice, once for the rows and once for the columns, as in Eq. (4). And the corresponding downsampling scheme is to keep the upper left corner matrix.

$$\mathbf{y} = \mathbf{W}\mathbf{x}\mathbf{W}^T \quad (4)$$

The invertibility of the transformation can be guaranteed by either the orthogonal or bi-orthogonal conditions on the transformation matrix (Van Fleet, 2011). However, one can also derive the invertibility through the lifting method used to implement fast wavelet transformation (Sweldens, 1998). The lifting method expresses the linear transformation (*e.g.* LeGall wavelet, Le Gall & Tabatabai (1988)) in the following form

$$\begin{aligned} d_k &= e_k - \lfloor (o_k + o_{k+1})/2 \rfloor \\ s_k &= o_k + \lfloor (d_{k-1} + d_k)/4 + 1/2 \rfloor \end{aligned} \quad (5)$$

The definition of d , s , e , and o is a way of partitioning vector y and x . *i.e.* $y = [s_0, d_0, s_1, d_1, \dots]$ and $x = [o_0, e_0, o_1, e_1, \dots]$. Eq. (5) can be written as two layers of NICE, as in Eq. (2), which is an invertible bijective mapping. A detailed deduction can be found in Appx. A.

3. Neural Wavelet Flow

In the following section, two ways of constructing two-dimensional learnable wavelet transformation are given. The first construction defines a learnable one-dimensional wavelet and applies it twice in two directions. The second directly defines a two-dimensional learnable wavelet transformation. Then, a corresponding training scheme is given.

3.1. One-dimentional

Building on the fact that wavelet transformations can be formulated as layers of normalizing flow transformations (Sec. 2.2), we can further generalize this idea to define a learnable one-dimensional wavelet transformation.

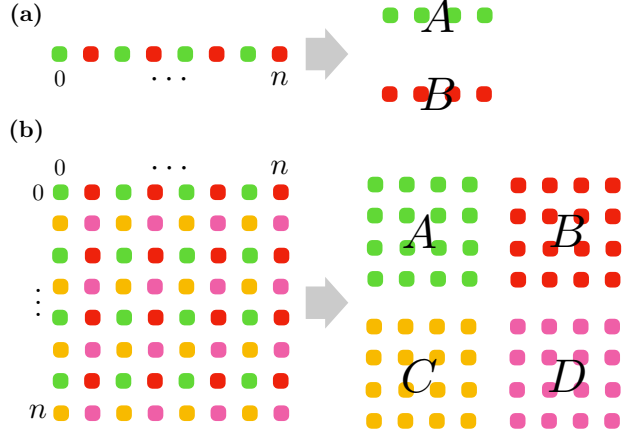


Figure 2. Variable partition in (a) one-dimensional case and (b) two-dimensional case.

For an n -variable one-dimensional vector data \mathbf{x} , we can divide it into two parts as diagramed in Fig. 2(a). The even-index variables are labeled A and odd-index variables are labeled B . Then Eq. (2) can be applied multiple times to iteratively update both A and B , as in NICE (Dinh et al., 2015). After transformation, the resulted variables in B are viewed as the output of the high-pass filters, and factored-out from later transformations. Variables in A are viewed as the output of the low-pass filters and passed to the next level of transformation. This partition, transformation, and factor-out process constitute one iteration of the learnable wavelet transformation. And the parameters controlling the transformation are shared in each iteration, to make sure the same high-pass/low-pass filter pairs are used. This scheme can be initialized to perform certain wavelets at the start. Appx. A demonstrates a way of initializing the transformations to be Haar wavelet (Haar, 1910) or LeGall wavelet (Le Gall & Tabatabai, 1988).

3.2. Two-dimentional

With one-dimensional wavelet transformation defined above, one simple way to define two-dimensional wavelet transformation is like in Eq. (4). As the learnable wavelet transformations are non-linear, transformation matrix \mathbf{W} is unknown. One way to circumvent this is to transpose the two-dimensional matrix \mathbf{x} instead of \mathbf{W} . *i.e.* we can treat rows of the matrix as batch and perform the learnable wavelet, then transpose the matrix and perform the learnable wavelet again on the batch of columns. At factor-out/downsampling phase, the variables corresponding to the low-pass results of rows and columns at the same time are kept. The

pseudocode of this process can be found in Appx. D.

Another proposed way utilizes a two-dimensional partition scheme, as diagramed in Fig. 2(b). In every 2×2 non-overlapping sub-matrix forming the original $n \times n$ matrix, the upper left, upper right, lower left, and lower right variables are labeled A , B , C , and D respectively. The A variables form a smaller $\frac{n}{2} \times \frac{n}{2}$ matrix, and so does B , C , D variables. Then the following transformation is performed to update variable A .

$$\begin{bmatrix} \mathbf{x}_A & \mathbf{x}_B \\ \mathbf{x}_C & \mathbf{x}_D \end{bmatrix}_k = \begin{bmatrix} \mathbf{x}_A + t([\mathbf{x}_B, \mathbf{x}_C, \mathbf{x}_D]) & \mathbf{x}_B \\ \mathbf{x}_C & \mathbf{x}_D \end{bmatrix}_{k-1} \quad (6)$$

t here maps concatenated variables $[\mathbf{x}_B, \mathbf{x}_C, \mathbf{x}_D]$ into the space of \mathbf{x}_A , *e.g.* convolutional networks with input channel 3 times the output channel. Three more transformations like this are performed to update B , C , and D in turn. This process can be applied multiple times to constitute a more expressive transformation.

For factor-out/downsampling, one of the four smaller matrices is considered results of the low-pass filters, *e.g.* \mathbf{x}_A , and kept as the input matrix of the next iteration. The rest three matrices \mathbf{x}_B , \mathbf{x}_C , and \mathbf{x}_D are considered the high-pass results and are factored-out. The pseudocode of the above process can be found in Appx. D.

3.3. Training

To train this learnable wavelet transformation, we perform the iterations defined above until no variables can be factored-out. The factored-out variables are considered from mutually independent distributions with learnable parameters, as diagramed in Fig. 3. And these distributions at different iterations also share parameters. To boost performance, the parameters of these distributions can be outputs of neural networks, as shown by the dashed line in Fig. 3. And these networks also share parameters at different iterations. Then, as a normalizing flow model, the expected probability of the input variables $p(\mathbf{x}_0)$ could be evaluated using Eq. (1). We can maximize this expected probability as the loss function, and perform gradient descent.

At each iteration, this optimization goal asks the network to transform and separate the variables to fit two different kinds of distributions. One kind of distribution is the mutually independent distributions for factored-out variables. As independent distributions, variables sampled from them share zero mutual information, thus a natural fit for high-frequency variables. The other distribution is a more complex one and allows long-range correlations. This could be seen when

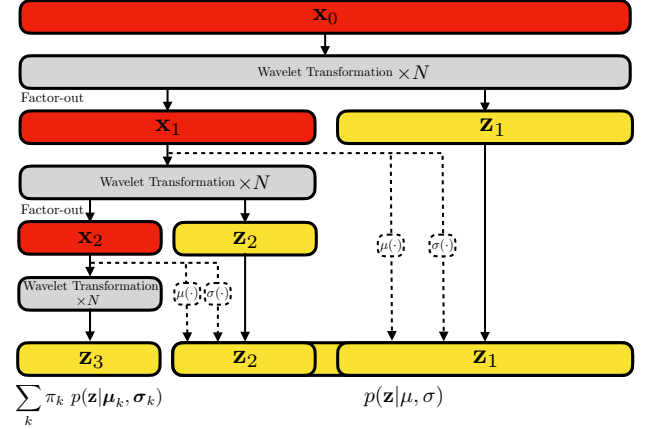


Figure 3. Network architecture. The red blocks are input variables of wavelet transformations of each iteration. The gray blocks are learnable wavelet transformations. At different iteration, they share the same parameters. The yellow blocks are factored-out variables. The dashed line shows optional neural networks for evaluating distribution parameters. They also share parameters at different iterations. The bottom blocks stand for the distributions of the transformed variables.

viewing Fig. 3 from bottom to top, inverting the flow and creating correlations between variables. This corresponding to the low-frequency variables. In this sense, the training process will result in high-pass/low-pass filter pairs. And the parameter-sharing scheme makes sure the low-pass distributions live in a corresponding space of the original physical space where the input lives, which also resembles the traditional wavelet transformations. A result of this correspondence can be seen in Fig. 1, where the low-pass variables resemble the original signal. This correspondence also makes generalizing these learned filters to samples with different dimensions possible, as they can be viewed as samples from different iterations.

For the last remaining variables, *e.g.* \mathbf{z}_3 in Fig. 3, we should use a more flexible class of probability distribution to allow the existence of long-range correlations. In this work, a mixture distribution (Kingma et al., 2016a; Salimans et al., 2017; Hooeboom et al., 2019) is in use for these last variables, the probability can be formulated as

$$p(\mathbf{z}|\boldsymbol{\mu}, \boldsymbol{\sigma}, \boldsymbol{\pi}) = \sum_k^K \pi_k \cdot p(\mathbf{z}|\boldsymbol{\mu}_k, \boldsymbol{\sigma}_k) \quad (7)$$

where K is the number of distributions in the mixture, and π_k , $\boldsymbol{\mu}_k$, and $\boldsymbol{\sigma}_k$ are the weight and parameters of the k -th distribution.

Table 1. Lossless compression scores(bits per dimension) on CIFAR-10, ImageNet32, ImageNet64. The scores in parenthesis are theoretical. The PNG, JPEF-2000, and FLIF scores are from Berg et al. (2020).

MODELS/ALGORITHMS	CIFAR-10	IMAGENET32	IMAGENET64
PNG (BOUTELL & LANE, 1997)	5.87	6.39	5.71
JPEG-2000 (RABBANI, 2002)	5.20	6.48	5.10
FLIF (SNEYERS & WUILLE, 2016)	4.19	4.52	4.19
LBB (HO ET AL., 2019)	3.12 (3.12)	3.88 (3.87)	3.70 (3.70)
IDF (HOOGEBOOM ET AL., 2019)	3.34 (3.32)	4.18 (4.15)	3.90 (3.90)
IDF++ (BERG ET AL., 2020)	3.26 (3.24)	4.12 (4.10)	3.81 (3.81)
NWF	3.59 (3.58)	4.02 (4.01)	3.74 (3.73)
NWF(IN YCbCr)	3.12 (3.10)	3.51 (3.50)	3.24 (3.24)

4. Experiment

In this section, applications of the learnable wavelet transformation are shown, including lossless compression, progressive loading, and super-resolution (upsampling). Then an analysis of the learned low-pass/high-pass filter pairs is given. The model in use is for discrete variables. And the second scheme defined in Sec. 3.2 is used, as it generally performs better. The t transformation networks in Eq. (6) utilize convolutional neural networks with input channel number three times the output channel. To make these networks work well with integers, the inputs are subtracted with 128 and divided by 255. And to make sure the output variables are discrete, the outputs of these networks are inverted into $0 \sim 255$, and rounded to the nearest integer (Hoogeboom et al., 2019; Berg et al., 2020). The distributions the inputs are mapped to are parameterized discrete logistic distributions, and the last one being the mixture of discrete logistic distributions (Hoogeboom et al., 2019; Salimans et al., 2017). For better performance, the optional networks for evaluating parameters of these distributions (dashed line in Fig. 3) are used. If not noted otherwise, datasets are converted to `uint8` RGB representation. More detailed structure descriptions and hyper-parameters can be found in Appx. C.

4.1. Lossless Compression

Lossless compression is a straightforward application for wavelet transformation (Rabbani, 2002; Charrier, 1999; Van Fleet, 2011). Recent works have shown it’s also a natural use case for normalizing flows (Hoogeboom et al., 2019; Berg et al., 2020), where the optimization goal happens to be minimizing the Shannon’s bound of lossless compression size (Shannon, 1948).

$$\mathbb{E}_x \text{Len}(\text{Code}(x)) \geq H(p) = -\mathbb{E}_x \log p(x) \quad (8)$$

To use the learnable wavelet in lossless compression, the routines are as follows. First, a learnable wavelet flow model defined as in Sec. 3 is trained using the max-

imizing probability scheme (minimizing the Shannon entropy). Then, samples are drawn from the dataset and transformed by the model to latent space variables. Finally, these latent variables can be compressed by entropy encoding algorithms (Huffman, 1952; Duda, 2009) according to their probabilities (entropies). Here, the entropy encoding algorithm in use is the rANS (Duda, 2009), which is introduced in Appx. B.

In Table 1, a compression score comparison of different models and algorithms on CIFAR-10 (Krizhevsky et al., 2009) and ImageNet32/64 (Chrabaszcz et al., 2017) dataset is given. The compression score in use is the bits per dimension (BPD), and are evaluated on the test set. For uncompressed image data, the BPD should be 8. To the best of the author’s knowledge, the learnable wavelet achieves better scores on ImageNet32/64 than the state-of-art normalizing-flow-based compression model (the IDF++ model, Berg et al. (2020)). And if convert these datasets into YCbCr space as in JPEG-2000 (Hamilton, 2004), this model achieves the best scores on CIFAR-10 and ImageNet32/64 than any models/algorithms reported in Table 1.

Next, a test of the model’s generalization ability is carried out. As shown in Table 2, the learned wavelet has satisfactory scores on datasets it’s not trained on. Due to the parameter-sharing scheme, the learned transfor-

Table 2. Compression scores on different datasets than trained on. The joint dataset is a combined dataset of CIFAR-10, ImageNet32, and ImageNet64. Scores are actual achieved BPDs.

EVALUATE ON	TRAIN ON		
	IMAGENET32	IMAGENET64	JOINT
CIFAR-10	3.81	3.76	3.73
IMAGENET32	4.02	4.05	4.09
IMAGENET64	3.75	3.74	3.80

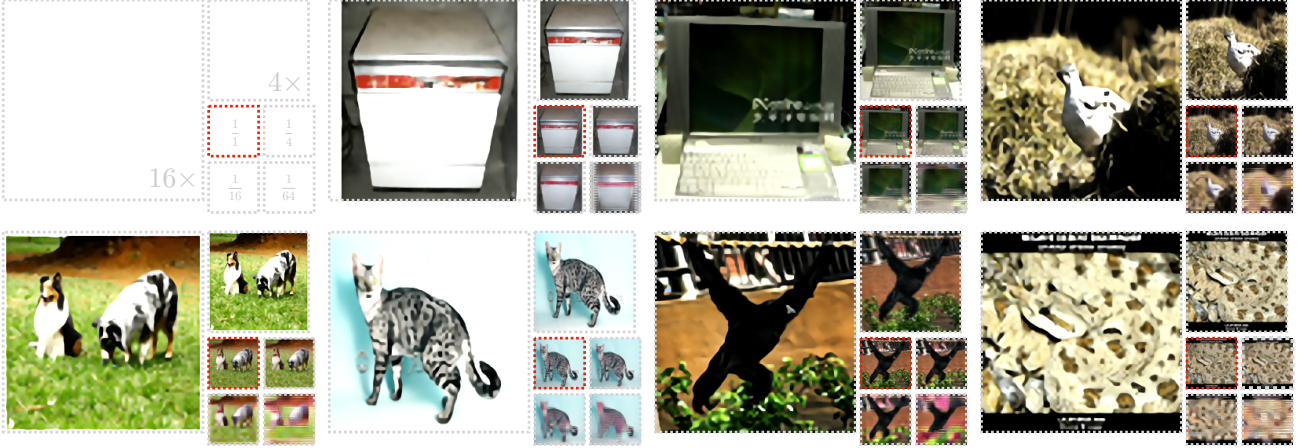


Figure 4. Progressive loading from 1/64, 1/16, and 1/4 original size back to the original size. And super-resolution of original images to 4 \times and 16 \times size. The layout is diagramed in the first plot. The images marked with red are the original images. The original images are from ImageNet64, and the model is trained on it.

mation puts no constrain on the input size. So, we can test ImageNet64 models on the ImageNet32 dataset. As in Table 2, the ImageNet64 model achieves nearly the same score on ImageNet32 as the model trained on it, and the same case for the ImageNet32 model on ImageNet64. This also implies a training scheme of training on small-dimension datasets and being used in the corresponding big-dimension datasets. This is a potential solution for the flow model’s dimension problem (Dinh et al., 2016). The generalization ability is also demonstrated in the compatibility of the datasets. The learnable wavelet relaxes the constrain of samples having the same size. So, a joint dataset of CIFAR-10 and ImageNet32/64 can be trained on. For the model trained on this joint dataset, the resulted scores are comparable with the models trained on each dataset.

4.2. Progressive Loading and Super-Resolution

Another straightforward application for wavelet is the progressive loading and super-resolution (upsampling) task. In both tasks, part of the image’s information is given, and the model is asked to fill out the rest pixels. The only difference being, for the progressive loading task, the ground truth (the original image) is known. So it’s more or less a lossy compression-reconstruction process. It’s also one of the improvements of JPEG-2000 over its predecessor (Rabbani, 2002; Charrier, 1999). In traditional wavelet use cases, this is also called upsampling.

To perform progressive loading/super-resolution using the neural wavelet flow, the procedures are as follows. A piece of low-pass variables is given (e.g. A of Fig. 2,

by first transforming the sample to latent space, and keep only this part of variables). As the model assume all high-pass variables (B , C , and D in Fig. 2) are from parameterized distributions, we can “gauss” the corresponding high-pass variables by drawing from these distributions. For models with parameter evaluation networks, the process is essentially the same, only that an evaluation of the parameters using the low-pass variables as input is performed firstly. Then, an inverse neural wavelet is performed to convert these variables back to the low-frequency variables space one iteration before. We can stop such iteration when reaches the desired size. A demonstration of progressive loading from 1/64, 1/16, and 1/4 original information back to the original size, and super-resolution of original images to 4 \times and 16 \times size is shown in Fig. 4. This demonstration is performed on ImageNet64, on which the model is also trained.

4.3. Numerical Analysis

In this section, a numerical analysis of the learned transformation is given to prove it’s composed of low-pass/high-pass filter pairs. The model in use here is trained on ImageNet64.

Firstly, with some normalizations, transformed variables at a certain iteration can be plot as an image. In Fig. 1, the model performs two iterations of the learned wavelet transformation on the classic Lena image. And the resulted variables, after subtracting distribution means (the zero points), are normalized to 0 \sim 1 float within each channel to visualize. The inner upper left corner of the upper left part of Fig. 1 is the low-pass

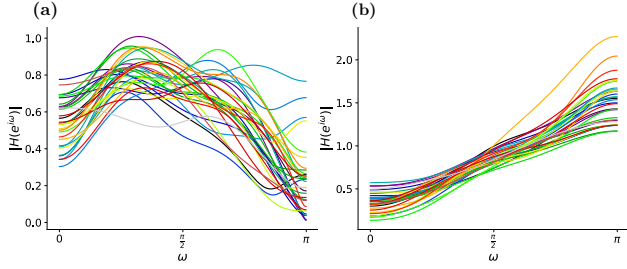


Figure 5. Plot (a) and (b) are frequency responses of learned low-pass filters and high-pass filters, respectively.

variables of the second iteration. As in traditional wavelet transformations, these low-pass variables can be viewed as a “blurred” version of the original signal (Van Fleet, 2011). And this “blurred” signal lives in a corresponding space of the original signal, thus still has physical meanings as the original signal. The same behavior can also be observed here. The rest inner corners of the upper left part are high-pass variables of the second iteration, and the upper right, down left, and down right parts are high-pass variables of the first iteration. In traditional wavelet, these variables corresponding to the high-frequency fine details of different levels in the original image (Van Fleet, 2011), we can also see this behavior here.

For traditional linear filters, a straightforward way of viewing its behavior is to plot its frequency response (Oppenheim, 1999). For the non-linear learned transformation, we can treat the gradient matrix of the output w.r.t. the input in a one-iteration transformation as a linear transformation matrix. And further, according to Eq. (4), we can get the transformation matrix \mathbf{W} as the output-row-to-input-row part of the gradient matrix. Then, this transformation matrix can be divided into high-pass/low-pass filters according to the definitions in Sec. 3.3. In this example, ImageNet64 samples are used. They have 64 rows, so there are 32 low-pass filters and 32 high-pass filters. In Fig. 5 (a) and (b), I plot the frequency responses of the learned low-pass and high-pass filters, respectively. Details of performing this plot can be found in Appx. C. We can see from the frequency responses of the low-pass filters, they demonstrate high responses around low to middle frequency, and relatively low responses at high frequency. As for the learned high-pass filters, they have responses that decreasing from high frequency to low frequency. These are typical behaviors for traditional linear low-pass/high-pass filters, respectively.

5. Related Work

As a normalizing flow model. This model can be viewed as a novel type of normalizing flow model. Comparing with the commonly used realNVP model (Dinh et al., 2016), the structural differences are as follows. This model partitions its variables in an unbalanced manner and updates them in a generalized lifting method way. This model also has a factor-out scheme, but also an unbalanced one like in the wavelet down-sampling. It shares parameters along the depth of the model, and factored-out variables are from mutually independent distributions.

As a learnable filter. One feature of this model is it’s learned filters. This aspect, in the world of deep learning, is more or less in line with disentangled representation works or non-linear ICAs. Similar works in terms of flow models include NICE (Dinh et al., 2015) and Sorrenson et al. (2020) which use volume-preserving transformations, NeuralRG (Li & Wang, 2018) and Hu et al. (2020b) which utilize the renormalization group concept from statistical physics, and Li et al. (2020) which uses harmonic analysis of classic mechanics.

As a lossless compression model. A major application demonstrated is the lossless compression task. There has been a series of works that connect flow models with lossless compression, including Hoogetboom et al. (2019) and Berg et al. (2020). The difference between them and the compression in this work is a swap of the model.

6. Conclusion

In this work, a novel kind of normalizing flow model is presented. This model extends linear wavelet transformation and proposes a scheme to learn non-linear wavelet transformation. As demonstrated in the paper, combined with the downstream task as an optimization goal, this model can achieve state-of-art results. Potential usage of this model including compression, progressive loading, super-resolution, ICA tasks, and multiple domain-specific cases that traditionally use wavelets. To the best of my knowledge, this is the first work that draws connections between normalizing flows and wavelet transformations.

References

- See <https://github.com/li012589/NeuralWavelet> for a PyTorch implementation of the code.
- See the Appendix for detailed discussion of initialization, experiment, and pseudocode, which cites

- Le Gall & Tabatabai 1988; Sweldens 1998; Dinh et al. 2015; Huffman 1952; Duda 2013; 2009; Hoogeboom et al. 2019; Kingma & Dhariwal 2018; Kingma & Ba 2014; Hamilton 2004; Van Fleet 2011; Reinhard et al. 2001.
- Amin, H. U., Malik, A. S., Ahmad, R. F., Badrud-din, N., Kamel, N., Hussain, M., and Chooi, W.-T. Feature extraction and classification for eeg signals using wavelet transform and machine learning techniques. *Australasian physical & engineering sciences in medicine*, 38(1):139–149, 2015.
- Ardizzzone, L., Lüth, C., Kruse, J., Rother, C., and Köthe, U. Guided image generation with conditional invertible neural networks. *arXiv preprint arXiv:1907.02392*, 2019.
- Berg, R. v. d., Gritsenko, A. A., Dehghani, M., Sønderby, C. K., and Salimans, T. Idf++: Analyzing and improving integer discrete flows for lossless compression. *CoRR*, 2020. URL <http://arxiv.org/abs/2006.12459v1>.
- Boutell, T. and Lane, T. Png (portable network graphics) specification version 1.0. *Network Working Group*, pp. 1–102, 1997.
- Canny, J. A computational approach to edge detection. *IEEE Transactions on pattern analysis and machine intelligence*, (6):679–698, 1986.
- Charrier, M. Jpeg2000: A new standard for still image compression. In *Multimedia Computing and Systems, International Conference on*, volume 1, pp. 9131–9131. IEEE Computer Society, 1999.
- Chen, L.-l., Zhao, Y., Zhang, J., and Zou, J.-z. Automatic detection of alertness/drowsiness from physiological signals using wavelet-based nonlinear features and machine learning. *Expert Systems with Applications*, 42(21):7344–7355, 2015.
- Chen, R. T. Q., Rubanova, Y., Bettencourt, J., and Duvenaud, D. Neural ordinary differential equations. *CoRR*, 2018. URL <http://arxiv.org/abs/1806.07366v5>.
- Chrabaszcz, P., Loshchilov, I., and Hutter, F. A down-sampled variant of imagenet as an alternative to the cifar datasets, 2017.
- Cruz, P., Mendes, A., and Magalhães, F. D. Using wavelets for solving pdes: an adaptive collocation method. *Chemical Engineering Science*, 56(10):3305–3309, 2001.
- Dinh, L., Krueger, D., and Bengio, Y. Nice: Non-linear independent components estimation, 2015.
- Dinh, L., Sohl-Dickstein, J., and Bengio, S. Density estimation using real nvp. *CoRR*, 2016. URL <http://arxiv.org/abs/1605.08803v3>.
- Donoho, D. L. Wavelet shrinkage and wvd: a 10-minute tour. In *Presented on the International Conference on Wavelets and Applications, Toulouse, France*, 1992.
- Donoho, D. L. and Johnstone, J. M. Ideal spatial adaptation by wavelet shrinkage. *biometrika*, 81(3): 425–455, 1994.
- Duda, J. Asymmetric numeral systems. *CoRR*, 2009. URL <http://arxiv.org/abs/0902.0271v5>.
- Duda, J. Asymmetric numeral systems: Entropy coding combining speed of huffman coding with compression rate of arithmetic coding. *CoRR*, 2013. URL <http://arxiv.org/abs/1311.2540v2>.
- Dugad, R., Ratakonda, K., and Ahuja, N. A new wavelet-based scheme for watermarking images. In *Proceedings 1998 International Conference on Image Processing. ICIP98 (Cat. No. 98CB36269)*, volume 2, pp. 419–423. IEEE, 1998.
- Figueiredo, M. A. Bayesian image segmentation using wavelet-based priors. In *2005 IEEE Computer Society Conference on Computer Vision and Pattern Recognition (CVPR’05)*, volume 1, pp. 437–443. IEEE, 2005.
- Haar, A. Zur theorie der orthogonalen funktionensysteme. *Mathematische Annalen*, 69(3):331–371, 1910. doi: 10.1007/BF01456326. URL <https://doi.org/10.1007/BF01456326>.
- Hamilton, E. Jpeg file interchange format. 2004.
- He, T., Wang, S., and Kaufman, A. Wavelet-based volume morphing. In *Proceedings Visualization’94*, pp. 85–92. IEEE, 1994.
- Ho, J., Lohn, E., and Abbeel, P. Compression with flows via local bits-back coding. *CoRR*, 2019. URL <http://arxiv.org/abs/1905.08500v3>.
- Hoogeboom, E., Peters, J. W. T., Berg, R. v. d., and Welling, M. Integer discrete flows and lossless compression. *CoRR*, 2019. URL <http://arxiv.org/abs/1905.07376v4>.
- Hu, H.-Y., Li, S.-H., Wang, L., and You, Y.-Z. Machine learning holographic mapping by neural network renormalization group. *Physical Review Research*, 2(2), Jun 2020a. ISSN 2643-1564. doi:

- 10.1103/physrevresearch.2.023369. URL <http://dx.doi.org/10.1103/PhysRevResearch.2.023369>.
- Hu, H.-Y., Wu, D., You, Y.-Z., Olshausen, B., and Chen, Y. Rg-flow: A hierarchical and explainable flow model based on renormalization group and sparse prior, 2020b.
- Huang, H., He, R., Sun, Z., and Tan, T. Wavelet-srnet: A wavelet-based cnn for multi-scale face super resolution. In *Proceedings of the IEEE International Conference on Computer Vision*, pp. 1689–1697, 2017.
- Huffman, D. A. A method for the construction of minimum-redundancy codes. *Proceedings of the IRE*, 40(9):1098–1101, 1952.
- Kingma, D. P. and Ba, J. Adam: A method for stochastic optimization. *arXiv preprint arXiv:1412.6980*, 2014.
- Kingma, D. P. and Dhariwal, P. Glow: Generative flow with invertible 1x1 convolutions. *CoRR*, 2018. URL <http://arxiv.org/abs/1807.03039v2>.
- Kingma, D. P., Salimans, T., Jozefowicz, R., Chen, X., Sutskever, I., and Welling, M. Improved variational inference with inverse autoregressive flow. In Lee, D., Sugiyama, M., Luxburg, U., Guyon, I., and Garnett, R. (eds.), *Advances in Neural Information Processing Systems*, volume 29, pp. 4743–4751. Curran Associates, Inc., 2016a. URL <https://proceedings.neurips.cc/paper/2016/file/ddeebdeefdb7e7e7a697e1c3e3d8ef54-Paper.pdf>.
- Kingma, D. P., Salimans, T., Jozefowicz, R., Chen, X., Sutskever, I., and Welling, M. Improved variational inference with inverse autoregressive flow. *Advances in neural information processing systems*, 29:4743–4751, 2016b.
- Krizhevsky, A., Hinton, G., et al. Learning multiple layers of features from tiny images. 2009.
- Le Gall, D. and Tabatabai, A. Sub-band coding of digital images using symmetric short kernel filters and arithmetic coding techniques. In *ICASSP-88., International Conference on Acoustics, Speech, and Signal Processing*, pp. 761–762. IEEE Computer Society, 1988.
- Li, S.-H. and Wang, L. Neural network renormalization group. *Phys. Rev. Lett.*, 121:260601, Dec 2018. doi: 10.1103/PhysRevLett.121.260601. URL <https://link.aps.org/doi/10.1103/PhysRevLett.121.260601>.
- Li, S.-H., Dong, C.-X., Zhang, L., and Wang, L. Neural canonical transformation with symplectic flows. *Phys. Rev. X*, 10:021020, Apr 2020. doi: 10.1103/PhysRevX.10.021020. URL <https://link.aps.org/doi/10.1103/PhysRevX.10.021020>.
- Mallat, S. and Hwang, W. L. Singularity detection and processing with wavelets. *IEEE transactions on information theory*, 38(2):617–643, 1992.
- Marr, D. and Hildreth, E. Theory of edge detection. *Proceedings of the Royal Society of London. Series B. Biological Sciences*, 207(1167):187–217, 1980.
- Noé, F., Olsson, S., Köhler, J., and Wu, H. Boltzmann generators: Sampling equilibrium states of many-body systems with deep learning. *Science*, 365(6457):eaaw1147, 2019.
- Oppenheim, A. V. *Discrete-time signal processing*. Pearson Education India, 1999.
- Paszke, A., Gross, S., Massa, F., Lerer, A., Bradbury, J., Chanan, G., Killeen, T., Lin, Z., Gimelshein, N., Antiga, L., Desmaison, A., Kopf, A., Yang, E., DeVito, Z., Raison, M., Tejani, A., Chilamkurthy, S., Steiner, B., Fang, L., Bai, J., and Chintala, S. Pytorch: An imperative style, high-performance deep learning library. In Wallach, H., Larochelle, H., Beygelzimer, A., d'Alché-Buc, F., Fox, E., and Garnett, R. (eds.), *Advances in Neural Information Processing Systems 32*, pp. 8024–8035. Curran Associates, Inc., 2019.
- Rabbani, M. Jpeg2000: Image compression fundamentals, standards and practice. *Journal of Electronic Imaging*, 11(2):286, 2002.
- Reinhard, E., Adhikhmin, M., Gooch, B., and Shirley, P. Color transfer between images. *IEEE Computer graphics and applications*, 21(5):34–41, 2001.
- Rezende, D. J. and Mohamed, S. Variational inference with normalizing flows. *arXiv preprint arXiv:1505.05770*, 2015.
- Salimans, T., Karpathy, A., Chen, X., and Kingma, D. P. Pixelcnn++: Improving the pixelcnn with discretized logistic mixture likelihood and other modifications. *arXiv preprint arXiv:1701.05517*, 2017.
- Shafiullah, M., Abido, M. A., and Al-Hamouz, Z. Wavelet-based extreme learning machine for distribution grid fault location. *IET Generation, Transmission & Distribution*, 11(17):4256–4263, 2017.
- Shannon, C. E. A mathematical theory of communication. *The Bell system technical journal*, 27(3):379–423, 1948.

- Sneyers, J. and Wuille, P. Flif: Free lossless image format based on maniac compression. In *2016 IEEE International Conference on Image Processing (ICIP)*, pp. 66–70. IEEE, 2016.
- Song, J., Zhao, S., and Ermon, S. A-nice-mc: Adversarial training for mcmc. In *Advances in Neural Information Processing Systems*, pp. 5140–5150, 2017.
- Sorrenson, P., Rother, C., and Köthe, U. Disentanglement by nonlinear ica with general incompressible-flow networks (gin), 2020.
- Sweldens, W. *Construction and applications of wavelets in numerical analysis*. PhD thesis, PhD thesis, Department of Computer Science, Katholieke Universiteit Leuven ..., 1994.
- Sweldens, W. The lifting scheme: A construction of second generation wavelets. *SIAM journal on mathematical analysis*, 29(2):511–546, 1998.
- Van Fleet, P. J. *Discrete wavelet transformations: An elementary approach with applications*. John Wiley & Sons, 2011.
- Williams, T. and Li, R. Wavelet pooling for convolutional neural networks. In *International Conference on Learning Representations*, 2018.
- Yousefzadeh, R. and Huang, F. Using wavelets and spectral methods to study patterns in image-classification datasets, 2020.
- Yu, J., Derpanis, K., and Brubaker, M. A. Wavelet flow: Fast training of high resolution normalizing flows. *Advances in Neural Information Processing Systems*, 33, 2020.
- Zhong, Z., Shen, T., Yang, Y., Lin, Z., and Zhang, C. Joint sub-bands learning with clique structures for wavelet domain super-resolution. *Advances in Neural Information Processing Systems*, 31:165–175, 2018.

A. The Generalized Lifting Method and Initialization of Haar/LeGall Wavelet

The 8×8 transformation matrix \mathbf{W} for the LeGall wavelet (Le Gall & Tabatabai, 1988) can be formulated as follows.

$$\mathbf{W}_{\text{legall}} = \begin{bmatrix} 3/4 & 1/2 & -1/4 & 0 & 0 & 0 & 0 & 0 \\ -1/8 & 1/4 & 3/4 & 1/4 & -1/8 & 0 & 0 & 0 \\ 0 & 0 & -1/8 & 1/4 & 3/4 & 1/4 & -1/8 & 0 \\ 0 & 0 & 0 & 0 & -1/8 & 1/4 & 5/8 & 1/4 \\ -1/2 & 1 & -1/2 & 0 & 0 & 0 & 0 & 0 \\ 0 & -1/2 & 1 & -1/2 & 0 & 0 & 0 & 0 \\ 0 & 0 & 0 & -1/2 & 1 & -1/2 & 0 & 0 \\ 0 & 0 & 0 & 0 & 0 & 0 & -1 & 1 \end{bmatrix} \quad (\text{A.1})$$

The corresponding transformation as follows,

$$\begin{bmatrix} 3/4 & 1/2 & -1/4 & 0 & 0 & 0 & 0 & 0 \\ -1/8 & 1/4 & 3/4 & 1/4 & -1/8 & 0 & 0 & 0 \\ 0 & 0 & -1/8 & 1/4 & 3/4 & 1/4 & -1/8 & 0 \\ 0 & 0 & 0 & 0 & -1/8 & 1/4 & 5/8 & 1/4 \\ -1/2 & 1 & -1/2 & 0 & 0 & 0 & 0 & 0 \\ 0 & -1/2 & 1 & -1/2 & 0 & 0 & 0 & 0 \\ 0 & 0 & 0 & -1/2 & 1 & -1/2 & 0 & 0 \\ 0 & 0 & 0 & 0 & 0 & 0 & -1 & 1 \end{bmatrix} \cdot \begin{bmatrix} v_1 \\ v_2 \\ v_3 \\ v_4 \\ v_5 \\ v_6 \\ v_7 \\ v_8 \end{bmatrix} = \begin{bmatrix} -v_3/8 + v_2/4 + 3v_1/4 + v_2/4 - v_3/8 \\ -v_1/8 + v_2/4 + 3v_3/4 + v_4/4 - v_5/8 \\ -v_3/8 + v_4/4 + 3v_5/4 + v_6/4 - v_7/8 \\ -v_5/8 + v_6/4 + 3v_7/4 + v_8/4 - v_7/8 \\ -v_1/2 + v_2 - v_3/2 \\ -v_3/2 + v_4 - v_5/2 \\ -v_5/2 + v_6 - v_7/2 \\ -v_7/2 + v_8 - v_7/2 \end{bmatrix} \quad (\text{A.2})$$

The corresponding low-pass filter of LeGall is defines as $(-1/8, 1/4, 3/4, 1/4, -1/8)$, and the high-pass filter is $(-1/2, 1, -1/2)$. The upper part of Eq. (A.2) is the low-pass results, and the lower part is the high-pass results.

Another way of performing this is through the lifting method (Sweldens, 1998), which uses a different partition scheme.

$$\begin{aligned} \mathbf{o} &= (v_1, v_3, v_5, v_7) \\ \mathbf{e} &= (v_2, v_4, v_6, v_8) \end{aligned} \quad (\text{A.3})$$

The high-pass results \mathbf{d} formulate as

$$\begin{aligned} d_k &= e_k - \lfloor (o_k + o_{k+1})/2 \rfloor \\ o_k &= o_k \end{aligned} \quad (\text{A.4})$$

And then, low-pass results \mathbf{s} can be computed using \mathbf{o} , \mathbf{e} , and \mathbf{d} , as follows.

$$\begin{aligned} d_k &= d_k \\ s_k &= o_k + \lfloor (d_k + d_{k-1})/4 \rfloor \end{aligned} \quad (\text{A.5})$$

These two equations can be formulated as a typical NICE (Dinh et al., 2015) transformation. So, as long we can provide t transformations serving as high-pass/low-pass filters, we can view NICE transformations as a generalized lifting method.

The Haar wavelet can also be formulated in this form,

$$\begin{aligned} d_k &= e_k - \lfloor o_k \rfloor \\ o_k &= o_k \\ d_k &= d_k \\ s_k &= o_k + \lfloor d_k/2 \rfloor \end{aligned} \quad (\text{A.6})$$

where \mathbf{d} and \mathbf{s} are high-pass results and low-pass results, respectively. The corresponding transformation matrix

is

$$\mathbf{W}_{\text{haar}} = \begin{bmatrix} 1/2 & 1/2 & 0 & 0 & 0 & 0 & 0 & 0 \\ 0 & 0 & 1/2 & 1/2 & 0 & 0 & 0 & 0 \\ 0 & 0 & 0 & 0 & 1/2 & 1/2 & 0 & 0 \\ 0 & 0 & 0 & 0 & 0 & 0 & 1/2 & 1/2 \\ -1 & 1 & 0 & 0 & 0 & 0 & 0 & 0 \\ 0 & 0 & -1 & 1 & 0 & 0 & 0 & 0 \\ 0 & 0 & 0 & 0 & -1 & 1 & 0 & 0 \\ 0 & 0 & 0 & 0 & 0 & 0 & -1 & 1 \end{bmatrix} \quad (\text{A.7})$$

Transformations Eq. (A.6), Eq. (A.4), and Eq. (A.5) can be converted into convolutional neural networks. However, the activation function ReLU eliminates negative values, which causes trouble. To circumvent this, we can use more than 6 channels, and distribute opposite values of the input on the other 3 channels. Then at the last layer, we remove the ReLU operation, and join these channels back.

For example, to init a LeGall wavelet flow, we write NICE transformations Eq. (2) as follows.

$$\begin{aligned} \mathbf{d} &= \mathbf{e} - \text{layer1}(\mathbf{o}) \\ \mathbf{o} &= \mathbf{o} \\ \mathbf{d} &= \mathbf{d} \\ \mathbf{s} &= \mathbf{o} + \text{layer2}(\mathbf{d}) \end{aligned} \quad (\text{A.8})$$

`layer1` and `layer2` are 1D convolutional networks with channel change $3 \rightarrow 10 \rightarrow 10 \rightarrow 3$. And `layer1` structured as

- (1) 1D replication padding two values on the right hand side.
- (2) `Conv1d(input_channel=3, outpur_channel=10, kernel_size=3, stride=1)`
- (3) `ReLU`
- (4) `Conv1d(input_channel=10, outpur_channel=10, kernel_size=3, stride=1, padding=1, padding_mode=replicate)`
- (5) `ReLU`
- (6) `Conv1d(input_channel=10, outpur_channel=3, kernel_size=3, stride=1, padding=1, padding_mode=replicate)`

The first (6, 3, 3) part of the weight for the first `Conv1d` is

$$\left[\begin{bmatrix} 0.5 & 0.5 & 0 \\ 0 & 0 & 0 \\ 0 & 0 & 0 \end{bmatrix}, \begin{bmatrix} 0 & 0 & 0 \\ 0.5 & 0.5 & 0 \\ 0 & 0 & 0 \end{bmatrix}, \begin{bmatrix} 0 & 0 & 0 \\ 0 & 0 & 0 \\ 0.5 & 0.5 & 0 \end{bmatrix}, \begin{bmatrix} -0.5 & -0.5 & 0 \\ 0 & 0 & 0 \\ 0 & 0 & 0 \end{bmatrix}, \begin{bmatrix} 0 & 0 & 0 \\ -0.5 & -0.5 & 0 \\ 0 & 0 & 0 \end{bmatrix}, \begin{bmatrix} 0 & 0 & 0 \\ 0 & 0 & 0 \\ -0.5 & -0.5 & 0 \end{bmatrix} \right]$$

The first (6, 6, 3) part of the weight for the second `Conv1d` is

$$\left[\begin{bmatrix} 0 & 1 & 0 \\ 0 & 0 & 0 \\ 0 & 0 & 0 \\ 0 & 0 & 0 \\ 0 & 0 & 0 \\ 0 & 0 & 0 \end{bmatrix}, \begin{bmatrix} 0 & 0 & 0 \\ 0 & 1 & 0 \\ 0 & 0 & 0 \\ 0 & 0 & 0 \\ 0 & 0 & 0 \\ 0 & 0 & 0 \end{bmatrix}, \begin{bmatrix} 0 & 0 & 0 \\ 0 & 0 & 0 \\ 0 & 1 & 0 \\ 0 & 0 & 0 \\ 0 & 0 & 0 \\ 0 & 0 & 0 \end{bmatrix}, \begin{bmatrix} 0 & 0 & 0 \\ 0 & 0 & 0 \\ 0 & 1 & 0 \\ 0 & 0 & 0 \\ 0 & 0 & 0 \\ 0 & 0 & 0 \end{bmatrix}, \begin{bmatrix} 0 & 0 & 0 \\ 0 & 0 & 0 \\ 0 & 0 & 0 \\ 0 & 1 & 0 \\ 0 & 0 & 0 \\ 0 & 0 & 0 \end{bmatrix}, \begin{bmatrix} 0 & 0 & 0 \\ 0 & 0 & 0 \\ 0 & 0 & 0 \\ 0 & 0 & 0 \\ 0 & 1 & 0 \\ 0 & 1 & 0 \end{bmatrix} \right]$$

The first $(3, 6, 3)$ part of the weight for the third Conv1d is

$$\begin{bmatrix} \begin{bmatrix} 0 & 1 & 0 \\ 0 & 0 & 0 \\ 0 & 0 & 0 \\ 0 & -1 & 0 \\ 0 & 0 & 0 \\ 0 & 0 & 0 \end{bmatrix}, \begin{bmatrix} 0 & 0 & 0 \\ 0 & 1 & 0 \\ 0 & 0 & 0 \\ 0 & 0 & 0 \\ 0 & -1 & 0 \\ 0 & 0 & 0 \end{bmatrix}, \begin{bmatrix} 0 & 0 & 0 \\ 0 & 0 & 0 \\ 0 & 1 & 0 \\ 0 & 0 & 0 \\ 0 & 0 & 0 \\ 0 & -1 & 0 \end{bmatrix} \end{bmatrix}$$

And the rest of the weights and all bias are set to zeros. **layer2** are defined similarly, with the only difference being changing the first 1D replication padding to the left-hand side. And the weights and bias are initialized the same as **layer1**, excepting the first $(6, 3, 3)$ part of the weight for the first Conv1d is initialized as

$$\begin{bmatrix} \begin{bmatrix} 0 & 0.25 & 0.25 \\ 0 & 0 & 0 \\ 0 & 0 & 0 \end{bmatrix}, \begin{bmatrix} 0 & 0 & 0 \\ 0 & 0.25 & 0.25 \\ 0 & 0 & 0 \end{bmatrix}, \begin{bmatrix} 0 & 0 & 0 \\ 0 & 0 & 0 \\ 0 & 0.25 & 0.25 \end{bmatrix}, \\ \begin{bmatrix} 0 & -0.25 & -0.25 \\ 0 & 0 & 0 \\ 0 & 0 & 0 \end{bmatrix}, \begin{bmatrix} 0 & 0 & 0 \\ 0 & -0.25 & -0.25 \\ 0 & 0 & 0 \end{bmatrix}, \begin{bmatrix} 0 & 0 & 0 \\ 0 & 0 & 0 \\ 0 & -0.25 & -0.25 \end{bmatrix} \end{bmatrix}$$

Defining a NICE transformation this way is equivalent to Eq. (A.4) and Eq. (A.5).

B. Entropy Encoding, ANS Compression and Normalizing Flow Compression Model

The intuitive understanding of entropy encoding as follows. The encoding process can be viewed as assigning a code string for each character. For a more frequently-apparent character, we assign a shorter code. Then the expected length is

$$\sum_x p(x)c(x) \quad (\text{B.1})$$

Then, this expectation is lower bounded by Shannon entropy Eq. (8). One straightforward way of achieving this kind of encoding is the Huffman encoding algorithm (Huffman, 1952), which uses a priority queue to sort the probabilities (frequencies) of characters. However, this implementation doesn't have a subtle discern of probability, only a two-pair comparison of probabilities. One more modern and better performing algorithm is the asymmetric numeral systems algorithm(ANS) (Duda, 2013; 2009). This algorithm expects a performance close to the Shannon entropy, and similar speed as Huffman encoding. For a state x , the character to encode s , and corresponding probability $p(s) \approx l_s/m$. The code C is

$$C(s, x) = m \lfloor x/l_s \rfloor + b_x + \text{mod}(x, l_s) \quad (\text{B.2})$$

where $b_x = \sum_{i=1}^{s-1} l_i$. Then, to decode from state x

$$D(x) = (s, l_x \lfloor x/m \rfloor + \text{mod}(x, m) - b_s) \quad (\text{B.3})$$

where s defined as $b_s \geq \text{mod}(x, m) < b_{s+1}$

One key point of entropy encoding is to assess a character's probability. This is where normalizing flows enter the picture. As they mapping distributions of data into tractable variable distributions with exact probabilities. Thus, they can be used to assess the characters' probabilities in the entropy encoding scheme. As pointed out by Hoogetboom et al. (2019).

C. Experiments Details

C.1. Structure Details and Hyper-parameters

The neural wavelet flow model in use has a **repeat** number of learnable wavelet transformations, where the **repeat** is a hyper-parameter. And the total number K of mixture distributions for the last factored-out variables is 5.

The structure of convolutional neural networks in use (for t networks and optional distribution-parameter-evaluation networks) are like in [Kingma & Dhariwal \(2018\)](#). The first and last ones are 3×3 , and the rest are 1×1 . The number of hidden layers (the 1×1 layers) is a controllable hyper-parameter `n_hidden`. The channels of these layers is also a hyper-parameter `hidden_channel`.

The optimizer is the Adamax ([Kingma & Ba, 2014](#)). And the learning rate is computed as in [Hoogeboom et al. \(2019\)](#), $lr = lr_{\text{base}} \cdot \text{decay}^{\text{epoch}}$.

Following Tab. C.1 gives detailed hyper-parameters for each case, all models used in the Sec. 4 can be found here.

Table C.1. Hyper-parameters for different datasets

Datasets	epoch	batchsize	repeat	n_hidden	hidden_channel	lr	decay
CIFAR-10	800	200	2	2	450	0.001	0.999
ImageNet32	800	200	3	3	350	0.001	0.99
ImageNet64	800	200	3	3	350	0.001	0.99
Joint	800	200	3	3	350	0.001	0.99
CIFAR-10(in YCbCr)	800	200	1	1	550	0.001	0.999
ImageNet32(in YCbCr)	800	200	3	3	350	0.001	0.99
ImageNet64(in YCbCr)	800	200	3	3	350	0.001	0.99

To prepare `uint8` RGB datasets, each sample is multiplied by 255 and rounding to the nearest `uint8` integer. For converting RGB dataset to YCbCr, this work uses the standard used in JPEG-2000 ([Hamilton, 2004](#)), which formulates as

$$\begin{bmatrix} Y \\ Cb \\ Cr \end{bmatrix} = \begin{bmatrix} 0.299 & 0.587 & 0.114 \\ -0.1687 & -0.3313 & 0.5 \\ 0.5 & -0.4187 & -0.0813 \end{bmatrix} \cdot \begin{bmatrix} R \\ G \\ B \end{bmatrix} + \begin{bmatrix} 0 \\ 128 \\ 128 \end{bmatrix} \quad (\text{C.1})$$

And the inverse transformation

$$\begin{bmatrix} R \\ G \\ B \end{bmatrix} = \begin{bmatrix} 1 & 0 & 1.402 \\ 1 & -0.34414 & -0.71414 \\ 1 & 1.772 & 0 \end{bmatrix} \cdot \begin{bmatrix} Y \\ Cb \\ Cr \end{bmatrix} + \begin{bmatrix} -172.456 \\ 135.45984 \\ -226.816 \end{bmatrix} \quad (\text{C.2})$$

The transformation from RGB to YCbCr and inverse are not invertible for `uint8` variables ([Van Fleet, 2011](#); [Hamilton, 2004](#)). After transformation, each variable is rounded to nearest `uint8` integer.

The dataset CIFAR-10 contains 50000 images and the test set contains 10000 images. ImageNet32 and ImageNet64 contain approximately 1250000 train images and 50000 test images. The joint dataset is a combined dataset of CIFAR-10, ImageNet32, and ImageNet64, the train set, and the test set contain all corresponding samples. A remaining samples counter is kept for each dataset, At sampling, a batch of samples is randomly drawn from one of the three datasets according to the normalized counter as probabilities. For each above datasets, a validation set that was held out from the respective training sets, but the training is done on the entire training set.

The hardware in use is $8 \times$ NVIDIA V100 GPUs. And the implementation of this model uses the Pytorch framework ([Paszke et al., 2019](#)).

C.2. Color Shift

One problem that may occur in the super-resolution task is the color shift. This is assumed to be a training unstable problem. It disappears when models are trained on big-dimension datasets, like ImageNet64. These big-dimension datasets take more iterations of transformation, and the training model has more depth of layers. Thus a better fit for the ideal situation mentioned in Sec. 3.3 (low-frequency parts have long-range correlations). While small-dimension datasets often result in leaning color shift as a bias. The solution, despite using a big-dimension dataset, is using color matching algorithms ([Reinhard et al., 2001](#)). One should also note, for any plot in the paper, the color matching fix **is not** applied.

C.3. Frequency Response Plot

As shown in Eq. (A.2), the gradient matrix contains the low-pass filter $(-1/8, 1/4, 3/4, 1/4, -1/8)$ at rows of the upper part, and the high-pass filter $(-1/2, 1, -1/2)$ at rows of the lower part. Similarly, the gradient matrix of one iteration of the learned wavelet transformation can be used to extract low-pass/high-pass filters. The process as follows. First, take the gradient matrix of one output row w.r.t. the corresponding input row. According to the partition scheme plotted in Fig. 2, the even-numbered rows are low-pass filters, and the odd-numbered rows are high-pass filters. These rows h can then be used to compute the frequency responses as follows.

$$|H(e^{i\omega})| = \sum_{n=0}^N h[n]e^{-i\omega n} \quad (\text{C.3})$$

The N here is the number of values in each row. And ω ranges from 0 to π .

D. Pseudocodes

Algorithm D.1 2D Neural Wavelet Transformation (Scheme 1)

Input: input variables \mathbf{x} , list of neural networks t
Initialize *FactorOut* as empty list
for $\text{size}(\mathbf{x})$ not equal 2×2 **do**
 Separate \mathbf{x} into *Upper* and *Lower* as in Fig. 2(a)
 Initialize counter i as 0
 repeat
 $i++$
 Initialize counter n as 0
 repeat
 $\text{Lower} = \text{Lower} - t[n](\text{Upper})$
 $\text{Lower} = \text{Lower} + t[n](\text{Upper})$
 $n++$
 until n equals $\text{len}(t)$
 Transpose \mathbf{x}
 until i equals 2
 Set \mathbf{x} equal *Upper* part of both the two iterations
 Append *FactorOut* with two iterations' *Lower* part of variables
end for

Algorithm D.2 2D Neural Wavelet Transformation (Scheme 2)

Input: input variables \mathbf{x} , list of neural networks t
Initialize *FactorOut* as empty list
for $\text{size}(\mathbf{x})$ not equal 2×2 **do**
 Separate \mathbf{x} into *UL*, *UR*, *DL* and *DR* as in Fig. 2(b)
 Initialize counter n as 0
 repeat
 $\text{UL} = \text{UL} + t[n](\text{UR}, \text{DL}, \text{DR})$
 $\text{UR} = \text{UR} + t[n](\text{UL}, \text{DL}, \text{DR})$
 $\text{DL} = \text{DL} + t[n](\text{UL}, \text{UR}, \text{DR})$
 $\text{DR} = \text{DR} + t[n](\text{UL}, \text{UR}, \text{DL})$
 $n++$
 until n equals $\text{len}(t)$
 Set \mathbf{x} equal *UL*
 Append *FactorOut* with $[\text{UR}, \text{DL}, \text{DR}]$
end for
